7C/2010G502

Cobalt Hexacyanoferrate as Cathode Material for Na^+ Secondary Battery

Masamitsu Takachi[1], Tomoyuki Matsuda1, and Yutaka Moritomo[1,2]

[1]Graduate School of Pure and Applied Science, University of Tsukuba, Tsukuba 305-8571, Japan
[2]TIMS, University of Tsukuba, Tsukuba 305-8571, Japan

1 Introduction

SIB is a promising candidate for the next-generation battery beyond the lithium ion secondary battery (LIB) with safe, environmentally friendly, and low-cost characteristics. The SIB device stores the electric energy utilizing the intercalation/deintercalation process of abundant Na^+ (Clark number = 2.63), instead of rare Li^+ (0.006), between the cathode and anode active materials. In this sense, the SIB is suitable for large-scale battery for stable use of the solar and/or window energies. So far, many researchers investigated the cathode materials for SIB. Recently, Komaba et al.[1] have found that hard carbon exhibits a repeatable Na^+ intercalation behavior, and demonstrated that a coin-type full SIB with hard carbon/$NaNi_{0.5}Mn_{0.5}O_2$ configuration exhibits a high capacity of more than 200 mAh/g (anode basis) and an average operating voltage of 3 V with a good cyclability.

Coordination polymers are promising cathode materials for LIB and SIB, due to their covalent and nanoporous host framework. Among them, Prussian blue analogues, $A_xM[Fe(CN)_6]_y$ (A and M are the alkali and transition metals, respectively), exhibit a three-dimensional (3D) jungle-gym-type host framework and cubic nanopores, 0.5 nm at the edge. (see inset of Fig. 1) Moritomo's group[2] synthesized a manganese hexacyanoferrate thin film, $Li_{1.32}Mn[Fe(CN)_6]_{0.83}3.5H_2O$, with high Li concentration (x = 1.32). They reported that the thin-film electrode exhibits a large capacity of 128 mAh/g and an average operating voltage of 3.6 V against Li, with a good cyclability. Recently, Goodenough's group[3] have reported Na^+ intercalation behaviors in a K-M-$Fe(CN)_6$ system (M = Mn, Fe, Co, No, Cu, Zn). However, their coulomb efficiency (= 60 % for M = Fe) is very low. The low efficiency suggests an irreversible redox process in addition to the reversible Na^+ intercalation/deintercalation process.

2 Experiment

Thin films of $Na_xCo[Fe(CN)_6]_{0.90}2.9H_2O$ (denoted as NCF90) were synthesized by electrochemical deposition on an indium tin oxide (ITO) transparent electrode under potentiostatic conditions at -0.50 V vs a standard Ag/AgCl electrode in an aqueous solution, containing 0.8 mM $K_3Fe(CN)_6$], 0.5 mM $Co(NO_3)2$, and 5.0 M $Na(NO_3)$. The chemical composition of the films was determined by the inductively coupled plasma (ICP) method and CHN organic elementary analysis. The thickness of the film was measured with a profilometer (Dektak3030). The typical film thickness was 1.1 μm. The grain structures of the films were investigated using scanning electron microscopy (SEM) images (TECHNEX Mighty-8). The films consist of crystalline grains with diameters of 400 nm.

The electrochemical properties of the NCF90 films were investigated in a beaker-type cell using of Na as the anode. The electrolyte used was 1 M $NaClO_4$ in propylene carbonate (PC). The active areas of the films were about 2.0 cm^2. The cut-off voltage was in the range of 2.0 to 4.0 V. The charge rate was fixed at 0.6 C. The mass of each film was measured using a conventional electronic weighing machine after the film was carefully removed from the ITO glass with a microspatula. The experimental error for the mass, and hence the capacity, is 10 \%.

The structural properties of the NCF90 films were investigated against x by {\it ex situ} XRD measurements at the PF 7C beamline of Photon Factory, KEK. The magnitude of x of the LCF90 films was controlled by the charge/discharge process in a beaker-type cell. We confirmed that the discharge capacity (= 135 mAh/g) of the NCF90 films was close to the ideal value (= 125 mAh/g). Then, the magnitude of x was calculated from the total current under the assumption that the fully discharged state is $Na_{1.6}Co[Fe(CN)_6]0_{.90}2.9HO$ (x = 1.6) and the fully charged state is $Co[Fe(CN)_6]0_{.90}2.9HO$ (x = 0.0). The films were carefully removed from the ITO glass with a microspatula in air atmosphere. The fine powder samples were filled into a 0.3 mmϕ glass capillary, and the capillary was sealed in vacuum. In the entire x-region, the films were stable in air at least for 1 h. The capillary was sealed and placed on the Debye-Scherrer camera. The powder diffraction patterns were detected with an imaging plate (IP). The exposure time was 5 min. The X-ray wavelength (= 0.73255 A) was calibrated by the lattice constant of standard CeO_2 powders.

3 Results and Discussion

Figure 1 shows discharge curves of NCF90 films measured at various rates. The discharge curve can be regarded as the open-circuit-voltage (OCV) curve, because no rate dependence was observed in this rate region (not shown). The observed capacity (= 135 mAh/g) is close to the ideal value (= 125 mAh/g) for the two-electron reaction. The discharge curve exhibits two plateaus at 3.8 (plateau I) and 3.4 V (plateau II). The thin film electrode exhibits a high capacity of 121 mAh/g

(90% of the OCV value) even at 60 C.

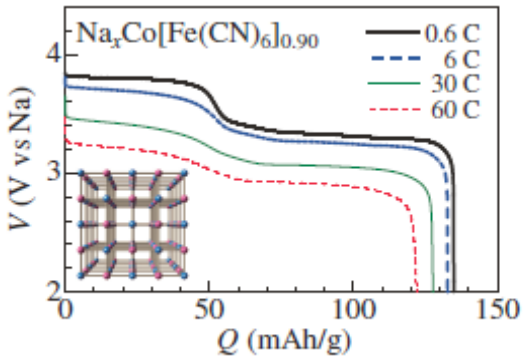

Fig. 1: (a) Discharge curves of NCF90 thin-film against x. (b) Lattice constant (a) of NCF90 against x. Open and closed circles denote data points obtained in the charge and discharge processes, respectively. Solid and broken lines in (b) indicate the results of the least-squares fittings in plateaus I and II, respectively...

Figure 2 shows the XRD patterns of NCF90 against x. We confirmed that all the reflections can be indexed with the face-centered cubic setting, as shown in parentheses The lattice constant (a) was refined by Rietveld analysis (Rietan-FP program) with the face-centered cubic model (Fm3m: Z = 4). In Fig. 3, we show the (a) discharge curve and (b) a of NCF90 against x. The magnitude of a slightly decreases in plateau I (0.0 < x < 0.6), while it steeply increases in plateau II (0.6 < x < 1.6). We estimated the x-coefficients (α = dlna/dx) of a in the respective plateaus [see the straight lines in Fig. 2(b)]: the magnitudes of α are - 0.1 and 2.4 \% in plateaus I and II, respectively.

Here, we discuss the redox reactions of the host framework in plateaus I and II.

The negative α (= - 0.3 %) observed in plateau I (= 3.8 V) suggests that the plateau is ascribed to the reduction process of Fe^{3+}. The negative α is probably due to the smaller size of $[Fe^{II}(CN)_6]^{4-}$ than that of $[Fe^{III}(CN)_6]^{3-}$. Furthermore, a similar negative α (= - 0.7 \%) is observed in the Fe redox region in manganese hexacyanoferrate, $Li_xMn[Fe(CN)_6]_{0.83}3.5H_2O$.[4] On the other hand, the large and positive α (= 2.4 %) observed in plateau II (= 3.4 V) is probably ascribed to the reduction process of the Co site from low-spin (LS) Co^{3+} to high-spin (HS) Co^{2+}. Because the larger ionic radius of the HS Co^{2+} (= 0.745 A) than of the LS Co^{3+} (= 0.545 A) well explains the observed lattice expansion. Igarashi et al.[5] investigated the valence state of $Na_xCo[Fe(CN)_6]_{0.90}2.9H_2O$ (0.75 < x < 1.60) by electrochemical treatment in an aqueous solution containing 1M NaCl. They found that the Co site changes from LS Co^{3+} to HS Co^{2+} with x. Consistently with the present case, the spin state transition of the Co site induces significant lattice expansion (α = 4.0 %).

In a simple electrochemical picture, it is apparently curious that the magnitude of V for the Fe reduction process (= 3.8 V; plateau I) is higher than that for the Co reduction process (= 3.4 V; plateau II). In addition, the magnitude of V (= 3.8 V) for plateau I is much larger than the redox voltage (= 3.07 V) for $[Fe(CN)_6]^{3-}/[Fe(CN)_6]^{4-}$ against Na/Na^+. These unexpected behaviors are ascribed to the strong coupling among charge, spin, lattice degree of freedoms in cobalt hexacyanoferrates. Reflecting the strong charge-spin-lattice coupling, $Na_xCo[Fe(CN)_6]_y$ takes two electronic states depending on the concentration (y) of $[Fe(CN)_6]$, i.e., HS Co^{2+} - LS Fe^{3+} state with large a and LS Co^{3+} - LS Fe^{2+} with small a. NCF90 (y = 0.90) corresponds to the latter case. We emphasize that, in the latter case, the Fe^{3+} state is more unstable than the Co^{3+} state. With this electronic structure, the reduction process from $N\_{x}Co^{3+}[Fe^{3+}(CN)_6]_y$ is expected to starts from unstable Fe^{3+} to stable Co^{3+}.Such an anomalous electronic structure is originated in the hybridization effect between Co and $[Fe(CN)_6]$, and is responsible for the significant deviation between the redox voltage (= 3.8 V) of $[Fe(CN)_6]^{3-}/[Fe(CN)_6]^{4-}$ in solid and that (= 3.07 V) in solution. The LS Co^{3+} - LS Fe^{2+} electronic configuration is reproduced by an ab initio band calculation[6] of ideal $NaCo[Fe(CN)_6]$ with use of experimentally-obtained atomic coordinates. The top of the valence band mainly consists of the Fed_6 (Fe^{2+}) state while the bottom of the conduction band consists of the Cod_7 (Co^{2+}) state.

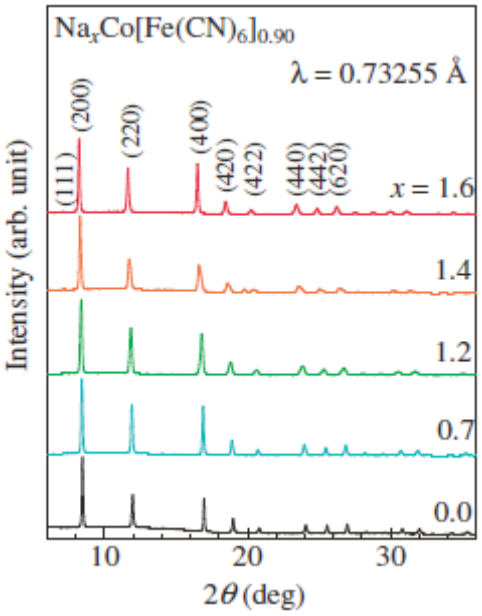

Fig. 2: XRD pattern of NCF90 against x. Values in parentheses represent indexes in the face-centered cubic setting.

Figure 3 shows examples of the XRD patterns of $Li_xNa_{0.13}Co[Fe(CN)_6]_{0.71}3.8H_2O$. We confirmed that the XRD patterns of all the compounds can be indexed with the face-centered cubic (Fm3m: Z = 4) setting, as shown in Fig. 3. The lattice constants (a) are plotted in Fig. 4 against x. Except for the Cd compound, a slightly decreases with increasing in x. The decrease in a is probably due to the smaller size of $[Fe^{II}(CN)_6]^{4-}$ than that

of $[Fe^{III}(CN)_6]^{3-}$. Actually, the Fe^{II} - N bond length (= 3.00 - 3.01 Å) is shorter than the Fe^{III} - N bond length (= 3.10 Å) in $RbMn[Fe(CN)_6]$. In the Mn compound, a decreases in the Mn redox region (x < 0.24).

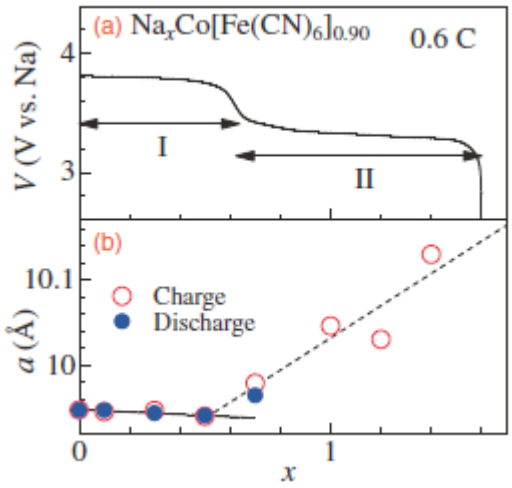

Fig. 3: (a) Discharge curves of thin-film electrode of NCF90 against x. (b) Lattice constant (a) of NCF90 against x. Open and closed circles denote data points obtained in the charge and discharge processes, respectively. Solid and broken lines in (b) indicate the results of the least-squares fittings in plateaus I and II, respectively.

Acknowledgement

This work was supported by a Grant-in-Aid (21244052) for Scientific Research from the Ministry of Education, Culture, Sports, Science and Technology. Elementary analysis was performed at Chemical Analysis Division, Research Facility Center for Science and Engineering, University of Tsukuba. The X-ray powder diffraction and X-ray absorption experiments were performed under the approval of the Photon Factory Program Advisory Committee (Proposal No. 2010G502).

References

[1] S. Komaba, W. Murata, T. Ishikawa, N. Yabuuchi, T. Ozeki, T. Nakayama, A. Ogata, K. Gotoh, and K. Fujiwara, Adv. Energy Mater,. **21** (2011) 3859.
[2] T. Matsuda and Y. Moritomo,ppl. Phys. Express, **4** (2011) 047101.
[3]Y. Lu, L. Wang, J. Cheng, and J. B. Goodenough, Chem. Commun., **48** (2012) 6544.
[4] T. Matuda and Y. Moritomo, J. Nanotechnol., **2012** (2012) 568147.
[5] K. Igarashi, F. Nakada, and Y. Moritomo. Phys. Rev. B **78** (2008) 235106.
[6] Y. Kurihara, H. Funashima, M. Ishida, N. Hamada, T. Matsuda, K. Igarashi, H. Tanida, T. Uruga, and Y. Moritomo, J. Phys. Soc. Jpn., **79**, (2010) 044710.

* pf-acr2012@kek.jp